

A TEMPLATE-PROPAGATION METHOD FOR SEGMENTATION OF FILAMENTOUS STRUCTURES IN ELECTRON TOMOGRAMS

Weicheng Shen*, Peijun Zhang[†], David Germain[†], Tracey Rouault[‡] and Sriram Subramaniam[†]

*SAIC, McLean, VA 22102, [†]NCI, [‡]NICHD, National Institutes of Health, Bethesda, Maryland 20892

ABSTRACT

We report a method for semi-automated segmentation of extended features such as filamentous structures in electron tomograms. We present an application of this method for the automatic propagation of segmented neurofilaments present along the axis of an axonal section of fixed, plastic-embedded mouse brain tissue imaged by three-dimensional electron microscopy. The algorithm uses the manually segmented features in a given slice to progressively extend the segmentation to successive slices based on knowledge of the centroids, shapes, and intensities of filaments in the previous slice. An iterative procedure allows for refinement of the most probable locations of the filaments in each slice. Evaluation of the performance of the propagation algorithm by visual inspection suggests that this approach can be used successfully for the rapid quantitative and statistical analysis of filamentous structures in cellular tomograms.

1. INTRODUCTION

Electron tomography provides new opportunities for the visualization of cellular and molecular assemblies that are too heterogeneous or complex to be studied by conventional methods such as X-ray crystallography or NMR spectroscopy [1]. The basic principles underlying 3D reconstruction using electron tomography are very similar to those used in techniques such as computerized axial tomography. Typically, a series of images of the object of interest are recorded by progressively varying the orientation of the specimen relative to the electron beam over a range of $\pm 70^\circ$. Reconstruction of the volume is then performed using a back-projection algorithm.

Electron tomograms recorded from biological specimens contain vast amounts of information about subcellular structure, but almost always display extremely low signal-to-noise ratios because of the low doses needed for imaging biological material. Interpretation of the complex features in electron tomograms therefore requires tedious manual segmentation. The development of semi-

automated approaches for segmentation with some level of user guidance is therefore highly desirable.

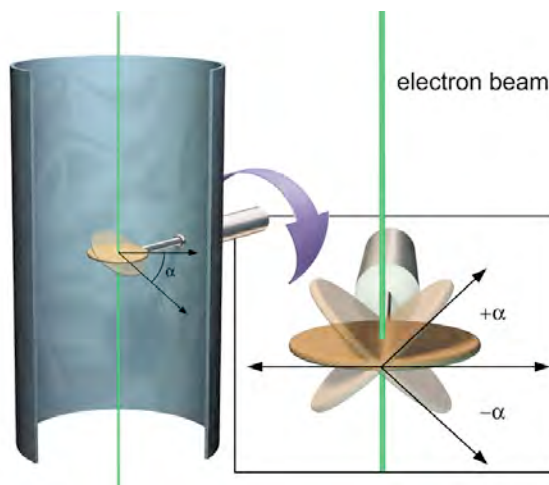


Fig. 1. Principle of varying the orientation of the specimen relative to the electron beam in an electron microscope.

As a first step in this direction, we describe the development of a method that uses the information present in a manually segmented slice of the tomogram and carries out automatic extension and refinement of segmentation for several successive slices. The method is especially applicable for the segmentation of features such as filaments and other extended objects where the features of interest typically persist over several slices of the tomogram.

For the data analyzed in this work, electron microscopic images were recorded on a Tecnai 12 microscope operating at 120 kV using mouse brain sections that had been fixed, stained and embedded in epon. Images recorded over a range of tilts were then combined using a back-projection algorithm to construct the three-dimensional density of the section. A single slice from a representative tomogram is shown in fig. 2.

2. SEGMENTATION ALGORITHM

Electron tomograms typically contain a hundred or more slices. The algorithm we have developed is designed to start with the information generated by the user in a single slice, and extrapolate the segmented contours from one slice to the next. It predicts the location of filaments image slice $k+1$ based on the centroids, shapes, and pixel values of the filaments objects of image slice k . The predictions are refined with the pixel values of image slice $k+1$, which results in the filaments segmentation map for image slice $k+1$. The accuracy of propagation is expected to fall gradually after several slices have been segmented, and this could be overcome by registration with periodic manual segmentation as needed. For the segmentation of filaments such as those shown in fig. 2, our procedure allows for propagation of segmentation over 20 slices without manual intervention.

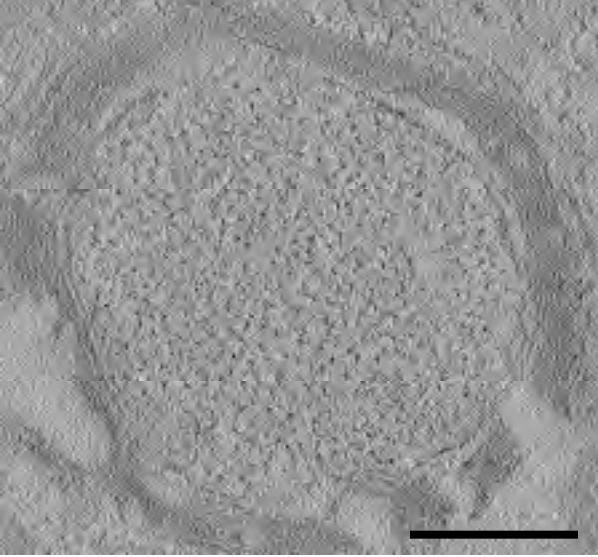


Fig. 2. A tomographic slice obtained from a 70 nm thick fixed, stained, and epon-embedded mouse brain section. The image shows the cross-sectional view through an axon; the myelin sheath surround the central region which is populated with filaments (seen as the dark spots) that run roughly along the axis of the axon. The scale bar is 1 micron wide.

3.1. Preprocessing

Since electron tomograms display very low signal-to-noise ratios, we perform anisotropic diffusion filtering [2] to smooth the image slices. The anisotropic diffusion equation used in this project is a modified version [3] of the one used by Perona and Malik [2]:

$$\frac{\partial I}{\partial t} = g(|\nabla G_{\sigma} * I|) |\nabla I| \operatorname{div} \frac{\nabla I}{|\nabla I|}$$

where $|\nabla I| \operatorname{div} \frac{\nabla I}{|\nabla I|}$ is a degenerate diffusion term that controls the diffusion directions, $g(|\nabla G_{\sigma} * I|)$ and is the “enhancement” term that controls the diffusion speed. It can be observed that the diffusion term only leads to diffusion of I in the direction orthogonal to that of ∇I , where I is the image and ∇I is the gradient of the image.

3.2. Extension of filament segmentation

We denote each image slice by I^k , where k is the slice index, and the entire stack of image slices is represented by the set $\mathcal{I} = \{I^1, I^2, \dots, I^N\}$. N is the total number of image slice in the stack. We define $F^k = \{f_1^k, f_2^k, \dots, f_{N_k}^k\}$ as the set of filaments at image slice k , where N_k is the number of filaments on image slice k , and f_j^k denotes the pixels in the connected component representing the j -th filament. If image slice k has already been segmented, the set $F^k = \{f_1^k, f_2^k, \dots, f_{N_k}^k\}$ is available for extrapolating the segmented 2D map of image slice k to image slice $k+1$. To produce the segmentation for image slice $k+1$, we first calculated the centroid of each connected component of $F^k = \{f_1^k, f_2^k, \dots, f_{N_k}^k\}$, which we refer to as $C^k = \{c_1^k, c_2^k, \dots, c_{N_k}^k\}$. Each c_j^k represents the coordinates of the centroid for f_j^k . Let $C^k = \{c_1^k, c_2^k, \dots, c_{N_k}^k\}$ be the set of initial estimates of the centroids for image slice $k+1$. For image I^{k+1} , we place a window centered at each centroid in the set $C^k = \{c_1^k, c_2^k, \dots, c_{N_k}^k\}$. We denote the window centered at c_j^k as w_j^{k+1} , and perform Otsu’s optimum thresholding [4] within w_j^{k+1} . The result of this operation within window w_j^{k+1} might create one or more connected components. We label these components as $g_1^j, g_2^j, \dots, g_{N_j}^j$, and denote this set of components as $G^j = \{g_1^j, g_2^j, \dots, g_{N_j}^j\}$, where g_p^j represents the pixels of p -th object of the thresholding result, and N_j is the total number of components after thresholding operation within window w_j^{k+1} . Based on various criteria, we can

select zero or more components from G^j as the segmentation extrapolation results on image slice $k + 1$ within window w_j^{k+1} . For segmenting filaments which are expected to persist (on average) through many slices, we

assume that no more than one object (f_j^{k+1}) on slice $k + 1$ can be extrapolated from the corresponding object (f_j^k) on slice k . The criterion of selecting one object, to be a candidate for f_j^{k+1} , from the set

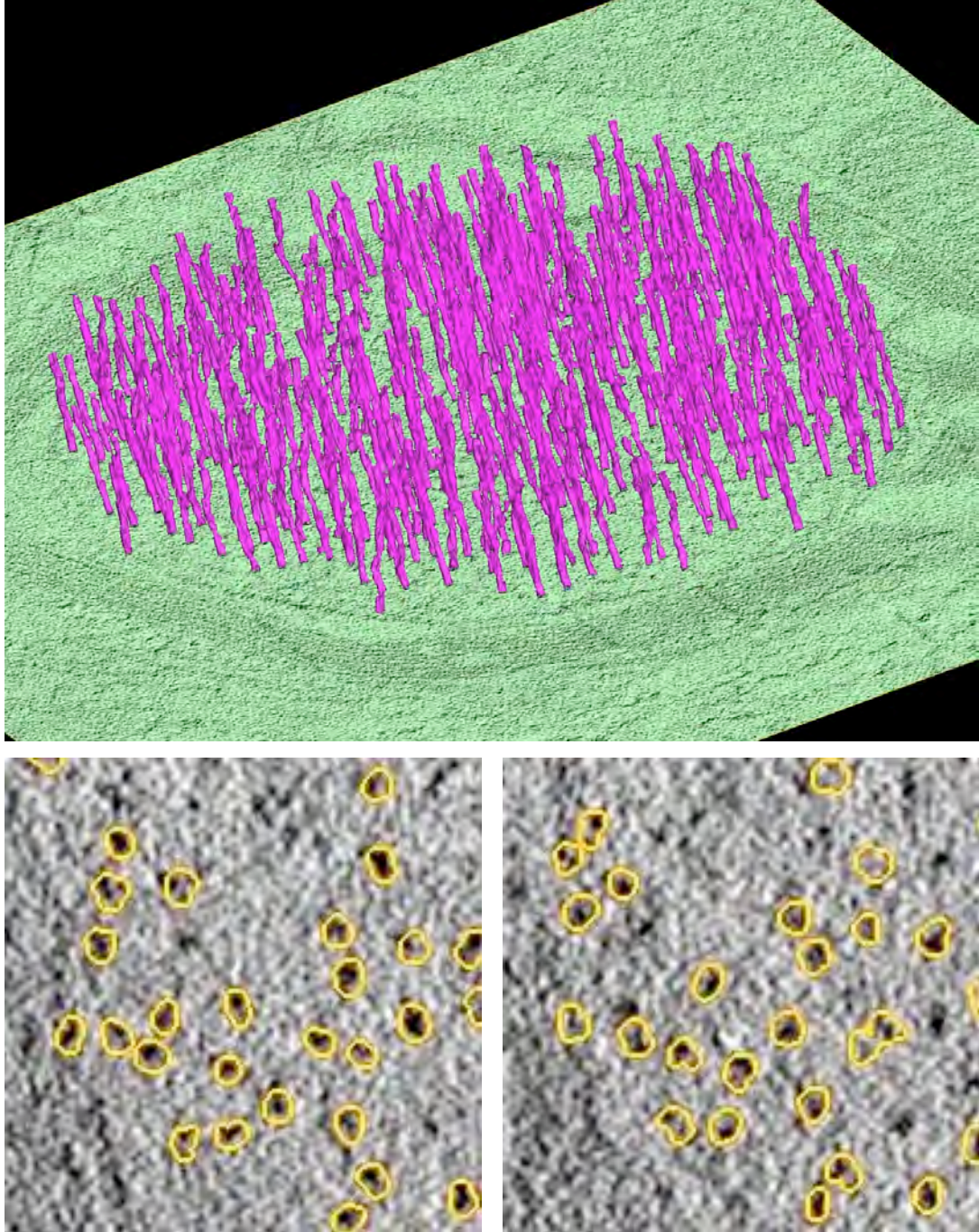


Fig. 3. Segmentation of filaments in the tomogram using the automated procedure described in this work. Only the first slice was segmented manually to identify the locations of the filaments. (a) 3D view of segmented region. (b, c) expanded views of a small region of the first (b) and fifteenth (c) slices generated automatically. It is evident that most of the filaments are correctly located even after propagation through fifteen slices.

$G^j = \{g_1^j, g_2^j, \dots, g_{N_j}^j\}$ is choosing the object that has the largest overlap with f_j^k . The overlap between any object g_p^j , $p \in \{1, 2, \dots, N_j\}$, and f_j^k is defined as $u_p^j = g_p^j \cap f_j^k$. As a result, a set of objects $U^j = G^j \cap f_j^k = \{u_1^j, u_2^j, \dots, u_{N_j}^j\}$ is produced. Let p be the index of the largest object in $U^j = \{u_1^j, u_2^j, \dots, u_{N_j}^j\}$. The object g_p^j is then denoted as f_j^{k+1} . The remaining objects in G^j are discarded (although some of them might be chosen under different criteria). Next, a morphological close operation with a disk shaped structure element is performed to smooth the shapes of the segmented structures. As a result, for each centroid c_j^k in C^k , a new object f_j^{k+1} is thus produced. Next the algorithm removes objects f_j^{k+1} , $j \in \{1, 2, \dots, N_k\}$, which are below a preset size threshold. After performing connected component labeling on the remaining set, a new set of filaments at image slice $k+1$, $F^{k+1} = \{f_1^{k+1}, f_2^{k+1}, \dots, f_{N_{k+1}}^{k+1}\}$ is generated, where N_{k+1} is the number of filaments on image slice $k+1$. This set of filaments can now be used for extrapolation of the segmentation to image slice $k+2$.

3. RESULTS

We tested the performance of this algorithm with a tomographic reconstruction of a sectioned slab obtained from mouse brain axon. The first slice of the tomogram was manually segmented in the environment of the program AMIRA (TGS Inc., San Diego) and used as the input for segmentation of the next 30 slices in the tomogram. A surface representation of the segmented 3D volume is shown in fig. 3a, with the unsegmented first slice displayed in the background. Visual inspection revealed that the segmentation had an excellent correspondence to the locations of the filaments in all slices. This point is illustrated in figs. 3b and 3c which show the automatically segmented features in two slices. Further, the performance of the algorithm after 15 slices of propagation (fig. 3c) is comparable to the performance observed in the first slice.

The results presented here can be extended to analyze tomograms more quantitatively, for example by classification of the filaments based on shape, length, width, density and texture. Each of these parameters could provide measures that would allow quantitative

correlation of cell and tissue architecture with biochemical and physiological investigations.

5. REFERENCES

- [1] S. Subramaniam and J. L. S. Milne "Three-dimensional electron microscopy at molecular resolution" *Ann. Rev. Biophys. and Biomol. Struct.*, vol. 33, June 2004 (in press).
- [2] P. Perona and J. Malik, "Scale space and edge detection using anisotropic diffusion", *IEEE Trans. Pattern Anal. Machine Intell.*, vol. PAMI-12, pp. 629-639, 1990.
- [3] L. Alvarez, P. Lions, and J. Morel, "Image selective smoothing and edge detection by nonlinear diffusion II", *SIAM J. Numer. Anal.*, vol. 29, No. 3, pp. 845-866, 1992.
- [4] N. Otsu, "A thresholding selection method from gray-level histogram", *IEEE Transactions on Systems, Man, and Cybernetics* 9(1): 62-66, 1979